Linear and nonlinear response of alkali-metal adlayers on metal surfaces to a static electric field

H. Ishida
Institute for Solid State Physics, University of Tokyo, 7-22-1 Roppongi, Minato-ku, Tokyo 106, Japan

A. Liebsch
Institut für Festkörperforschung, Forschungszentrum Jülich, D-5170 Jülich, West Germany
(Received 22 March 1990)

The linear and nonlinear response of alkali-metal adlayers on metal surfaces to a static electric field is studied within the local-density-functional theory as a function of the adatom coverages. Hexagonal Na layers with varying lattice constants are used as adlayers, and the metal substrate is represented by the semi-infinite jellium. The predictions of these first-principles electronic-structure calculations are compared with those of quasi-one-dimensional models where the positive ions of the alkali-metal adlayer are represented by a thin jellium model. For coverages above the work-function minimum, the linear and nonlinear response properties, which depend on the lateral average of the induced electronic density, are remarkably similar in both calculations. In particular, the position of the image plane and the nonlinear moment which determines the perpendicular second-harmonic surface polarization, are well reproduced within the jellium-on-jellium model. At coverages less than the work-function minimum, this model ceases to be realistic and the response properties strongly reflect the atomic character of the adsorbate.

I. INTRODUCTION

Alkali-metal adlayers on metal surfaces show a number of important electronic properties such as the large work-function decrease and the promotion of catalytic reactions.[1-3] The linear and nonlinear response properties of the adlayers are especially interesting since they determine several quantities observed in a variety of surface spectroscopies. In electron energy-loss experiments, a strong loss peak characteristic of the adlayer has been detected for a wide range of coverages Θ (number density of adatoms per unit area).[4-8] On the one hand, the peak is interpreted as due to the interband transition between the alkali-metal atom s- and p_z-derived states. On the other hand, it is attributed to a plasmon in the adlayer which becomes metallic at higher Θ. At present, there is no clear understanding of the nature of this excitation. Recently, it was observed that small amounts of alkali-metal atoms on Rh and Ag surfaces greatly enhance the efficiency of optical second-harmonic generation (SHG).[9,10] For full monolayers, the signal is several orders of magnitude larger than that of the clean surface. A qualitative explanation of this effect was proposed by Tom *et al.*[9] They invoked intra-atomic transitions between adatom resonances at lower Θ, whereas they emphasized the role of an interface plasmon at higher Θ. With the aim of analyzing the low-coverage region, Persson and Dubois[11] calculated the SHG using the model of Muscat and Newns,[12] which ignores the overlap of adatom orbitals. Liebsch,[13] on the other hand, studied the dynamical response of adsorbed alkali-metal monolayers within the time-dependent density-functional approach,[14-16] and showed that the SHG intensity is increased up to 3 orders of magnitude when the harmonic frequency satisfies a resonant condition of a collective mode at the adlayer-vacuum interface. He also analyzed recent optical reflectivity spectra for cesiated Ag surfaces[17] which show a characteristic variation with Cs coverage. Since in both calculations the adlayer was represented by a jellium slab, the model only describes the properties related to the density gradients normal to the surface and it ignores the effect of interband and atomiclike transitions.

To achieve a systematic understanding of the response properties of alkali-metal adlayers at low as well as high Θ, it is clearly necessary to have a theory which can describe both intra-atomic transitions and interband and collective excitations. A scheme which accurately describes the ground-state electronic properties of adsorbed alkali-metal layers at varying coverages has recently been presented by Ishida *et al.*[18-21] These first-principles calculations provided for the first time a quantitative picture of the charge rearrangement near the alkali-metal atoms as the coverage is decreased from a full monolayer to $\Theta \approx 0.2$.

As a first step towards the extension of this scheme to the description of dynamic response properties of alkali-metal adlayers, we have calculated the linear and nonlinear surface charge distributions induced by a static electric field (low-frequency limit). Particular emphasis is given to the question as to how the nature of the response varies as the adlayer changes from metallic to atomiclike with decreasing Θ. To illustrate this transition, we use hexagonal Na lattices with varying lattice constants as

adsorbates and represent the metallic substrate by a semi-infinite jellium system corresponding to the free-electron density of Ag. This substrate density was chosen in order to be able to compare with the previous work by Weber and Liebsch.[22] Results for Al ($r_s=2$) as substrate are qualitatively similar. We also have performed analogous response calculations using the two-step jellium model of Lang[23] in which the positive ions of the adlayer are replaced by a thin slab whose density is proportional to the coverage. This model is known to reproduce the measured variation of the work function with Θ remarkably well. An important result of the present work is that those linear and nonlinear response properties which depend only on the planar average of the induced density, are nearly identical for the discrete-adlayer-on-jellium and jellium-on-jellium models as long as the coverage is above the work-function minimum. This is so in spite of the fact that actual induced densities exhibit considerable atomic character within the adlayer. In this range of coverages, the full calculations therefore confirm the earlier static response calculations by Weber and Liebsch[22] carried out within the two-step jellium model. On the other hand, at coverages below the work-function minimum the atomic character is so dominant that this model becomes inappropriate.

The electronic structure of adatoms under the influence of a static electric field is important not only as the low-frequency limit of the response properties. It is also directly related to areas such as field ion microscopy and field-induced desorption. The present study is the first one that determines nonempirically the electronic structure of adatoms in the presence of a static electric field.

The outline of this paper is as follows: In Sec. II we present the model for the chemisorption of alkali-metal layers on a metallic substrate and discuss the method used to evaluate their electronic properties. In Sec. III we present the results of our calculations for the ground state, the linear response regime, and the nonlinear response regime. A summary is given in Sec. IV.

II. MODEL AND METHOD OF CALCULATION

Our model is an extension of the work of Lang and Williams[24] on the single-atom chemisorption on jellium to finite coverages. We calculate the electronic structure of the alkali-metal adlayers on the semi-infinite jellium within the local-density-functional approach[25] following the method of Ishida.[20] The method is a fully three-dimensional one and the presence of the semi-infinite substrate is taken into account by using the embedding approach of Inglesfield.[26] Figure 1 depicts the calculational geometry. Only the embedded region with $b_1 \le z \le b_2$ is explicitly treated, and the effects of the bulk jellium ($z < b_1$) and vacuum ($z > b_2$) are expressed in terms of complex embedding potentials acting on the two embedding surfaces at $z=b_1$ and $z=b_2$.

To describe one-electron wave functions and their logarithmic derivatives at the embedding surfaces, the Green function $G(\mathbf{r},\mathbf{r}',\varepsilon,\mathbf{k},\Theta,\sigma)=\langle \mathbf{r}|[\varepsilon+i\delta - H(\mathbf{k},\Theta,\sigma)]^{-1}|\mathbf{r}'\rangle$ is expanded in terms of the nonorthogonal basis set

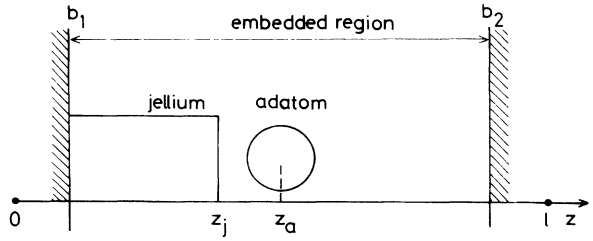

FIG. 1. Calculational geometry for alkali-metal adlayers on the semi-infinite jellium.

$$\phi_{\mathbf{k}+\mathbf{G},n}(\mathbf{r})=\left[\frac{2}{Sl}\right]^{1/2}\exp[i(\mathbf{k}+\mathbf{G})\cdot\mathbf{x}]\sin(k_n z) \quad (b_1 \le z \le b_2), \quad (1)$$

where $k_n=n\pi/l$ ($n>0$), S is the surface area, σ is a parameter for the electric field which will be explained later, and $\mathbf{k}$ and $\mathbf{G}$ denote the two-dimensional wave vector and reciprocal lattice vector, respectively. The matrix element of the energy-dependent embedding potential at $z=b_1$ is given by

$$H_{b_1}(\mathbf{k}+\mathbf{G},n;\mathbf{k}+\mathbf{G}',n') = \frac{1}{l}[(\mathbf{k}+\mathbf{G})^2-2\varepsilon]^{1/2}\sin(k_n b_1)\sin(k_{n'} b_1)\delta_{\mathbf{G},\mathbf{G}'}, \quad (2)$$

where the one-electron energy ε is measured from the bottom of the jellium potential, and the imaginary part of H_{b_1} is chosen negative[27] if $2\varepsilon > (\mathbf{k}+\mathbf{G})^2$ (we use atomic units with $m=e=\hbar=1$). The matrix element of the embedding potential at $z=b_2$ is obtained by replacing ε in Eq. (2) by $\varepsilon-\varepsilon_{\text{vac}}$, and also b_1 by b_2, where ε_{vac} is the potential barrier at $z=b_2$, which is determined self-consistently. The other matrix elements of the Hamiltonian are evaluated in a similar way as in standard slab calculations. We use the norm-conserving pseudopotential[28] for the adatom.

The new point in the present calculational procedure is to include the uniform electric field perpendicular to the surface. It is applied by placing a charge sheet at the plane $z=b_2$. The strength of the field E_{ap} is related to the sheet charge per unit area, σ, via $E_{\text{ap}}=2\pi\sigma$. For a given field, the charge density is calculated from the expression

$$n(\mathbf{r},\Theta,\sigma)=-\frac{1}{\pi}\int\frac{2\,d\mathbf{k}}{(2\pi)^2}\int^{E_F} d\varepsilon\,\mathrm{Im}G(\mathbf{r},\mathbf{r},\varepsilon,\mathbf{k},\Theta,\sigma), \quad (3)$$

and, corresponding to the basis set Eq. (1), it is expanded as

$$n(\mathbf{r},\Theta,\sigma)=\sum_{\mathbf{G}}\sum_{m\ge 0} n(\mathbf{G},m,\Theta,\sigma)\exp(i\mathbf{G}\cdot\mathbf{x})\cos(k_m z) \quad (b_1 \le z \le b_2). \quad (4)$$

Since the embedding method assumes no charge neutrality, the iteration procedure to self-consistency automatically finds an appropriate amount of screening charge which shields the external field in the bulk. The simple mixing of the input and output charge densities does not lead to convergence of the screening charge. We, therefore, use the higher-dimensional Anderson procedure reformulated in the language of the quasi-Newton method by Blügel.[29] In the actual calculation, the cut-off energy for the basis set Eq. (1) is chosen as 5 Ry, and b_1, z_j, b_2, and l (see Fig. 1) are set equal to 2, 10, 24, and 26 a.u., respectively.

We study hexagonal Na adlayers on the semi-infinite jellium with $r_s=3$ corresponding to the free-electron density of Ag. For the sake of comparison, we perform a set of parallel calculations for thin jellium adlayers. Following Weber and Liebsch,[22] we define the jellium slab with thickness $d_j=5.654$ a.u. and $r_s=4$ (positive background density $n_j=0.00373$ a.u.) as a full monolayer ($\Theta=1$). The thickness is chosen as a lattice spacing between close-packed layers of the bcc Na. For lower Θ, d_j is fixed at the monolayer value, and $n_j(\Theta)$ is varied as $n_j(\Theta)=\Theta\cdot n_j(\Theta=1)$. The lattice constant of the corresponding hexagonal Na adlayer at Θ, $a_\parallel$, is determined by the condition that the real and jellium adlayers should have the same number of electrons in the surface, i.e., $a_\parallel^2=2/[\sqrt{3}d_j n_j(\Theta)]$. The calculations are performed for $\Theta=1$, $\frac{3}{4}$, $\frac{1}{2}$, $\frac{1}{3}$, and $\frac{1}{5}$. The lattice constants $a_\parallel$ for these adlayers are 7.399, 8.544, 10.464, 12.816, and 16.545 a.u., respectively.

Another parameter is the distance between the Na core and jellium edge, z_a-z_j. It is set equal to $d_j/2=2.827$ a.u. for all Θ. A separate total-energy calculation for the hexagonal Na adlayers with $a_\parallel=9.35$ a.u. gave a value of 2.7 a.u. for the equilibrium Na-jellium distance, and it is expected that the Na adlayer shows a small outward relaxation with increasing Θ due to the weakening of the adatom-substrate bonding.[19] However, since the relaxation is small compared with the orbital size of Na, the adatom electronic structure changes only little within this relaxation length. Thus our value of 2.827 a.u. may be reasonable for the whole Θ range.

In the presence of a static electric field, the electron density can be expanded as[30]

$$n(\mathbf{r},\Theta,\sigma)=n_0(\mathbf{r},\Theta)+\sigma n_1(\mathbf{r},\Theta)+\sigma^2 n_2(\mathbf{r},\Theta)+\cdots , \tag{5}$$

where $n_0(\mathbf{r},\Theta)$, $n_1(\mathbf{r},\Theta)$, and $n_2(\mathbf{r},\Theta)$ are the ground-state, linear-induced, and second-order-induced charge densities, respectively. For each Θ, we perform three self-consistent calculations for $n_0(\mathbf{r},\Theta)$, $n_+(\mathbf{r},\Theta)$, and $n_-(\mathbf{r},\Theta)$, where $n_+(\mathbf{r},\Theta)$ and $n_-(\mathbf{r},\Theta)$ are the electron densities with a slightly positive or negative surface charge $\sigma(E_{\rm ap}=\pm 0.002$ a.u. in the actual calculations). Then $n_1(\mathbf{r},\Theta)$ and $n_2(\mathbf{r},\Theta)$ are obtained by

$$n_1(\mathbf{r},\Theta)=\frac{1}{2\sigma}[n_+(\mathbf{r},\Theta)-n_-(\mathbf{r},\Theta)] , \tag{6}$$

and

$$n_2(\mathbf{r},\Theta)=\frac{1}{2\sigma^2}[n_+(\mathbf{r},\Theta)+n_-(\mathbf{r},\Theta)-2n_0(\mathbf{r},\Theta)] . \tag{7}$$

In the static limit, the screening of the external electric field is perfect, and $n_1(\mathbf{r},\Theta)$ and $n_2(\mathbf{r},\Theta)$ should satisfy

$$\frac{1}{S}\int d\mathbf{r}\, n_1(\mathbf{r},\Theta)=1 , \tag{8}$$

and

$$\frac{1}{S}\int d\mathbf{r}\, n_2(\mathbf{r},\Theta)=0 . \tag{9}$$

III. RESULTS AND DISCUSSION

A. Ground state

Although we study in the present work the surface response by solving the Kohn-Sham equations[25] for the adlayers under a static field directly, an alternative way is to use the surface response functions constructed from the Green function of the ground state. In the latter approach, the response is described as due to virtual excitations from the occupied to unoccupied states of the ground state. In this sense, it is useful to examine ground-state electronic properties.

Figure 2 shows contour maps of the ground-state charge density $n_0(\mathbf{r},\Theta)$ for several Na coverages. In the direction along the surface, the density can be seen to vary appreciably with Θ. The outermost density contours at $\Theta=1$ are mostly parallel to the surface, while at $\Theta=\frac{1}{5}$, they protrude to the vacuum side so that the adlayer density is highly corrugated. Perpendicular to the surface, the charge distribution seems to depend rather weakly on Θ: The alkali-metal-atom valence charge, which acts as electron cloud that screens the positive ion cores of the adatoms, is always polarized ~ 1 a.u. toward the metal side of the Na nuclei. The degree of polarization does, however, depend sensitively on Θ.

This effect can be seen more clearly in Fig. 3, where the lateral average of the Na-induced ground-state valence charge $[\bar{n}_0(z,\Theta)-\bar{n}_0(z,\Theta=0)]/\Theta$ is plotted. Here $\bar{n}_0(z,\Theta)=\int d\mathbf{x}\, n_0(\mathbf{r},\Theta)/S$ is the planar average of $n_0(\mathbf{r},\Theta)$, and the normalization ensures that all distributions have unit area. For $\Theta=\frac{1}{5}$, $\frac{1}{3}$, $\frac{1}{2}$, $\frac{3}{4}$ and 1, the centroids $z_0(\Theta)$ of these screening clouds are located at 0.63, 0.45, 0.25, 0.11, and 0.05 a.u. on the metal side of the plane of Na atoms, respectively. Note that these centroids lie much closer to the plane of Na nuclei than the maxima of the density distributions. Qualitatively these curves resemble the screening charge distribution induced at the bare-jellium substrate by a purely external electric field (see dot-dashed curve).[31] The centroid of the latter distribution, which defines the position of the image plane, is located at 1.35 a.u. from the jellium edge, i.e., it lies at the distance $d=2.83-1.35=1.48$ a.u. on the metal side of the Na nuclei.

Since at the lowest Θ, the Na valence charge is highly asymmetric and slanted towards the metal, one may conclude that the Na valence electron has been partly

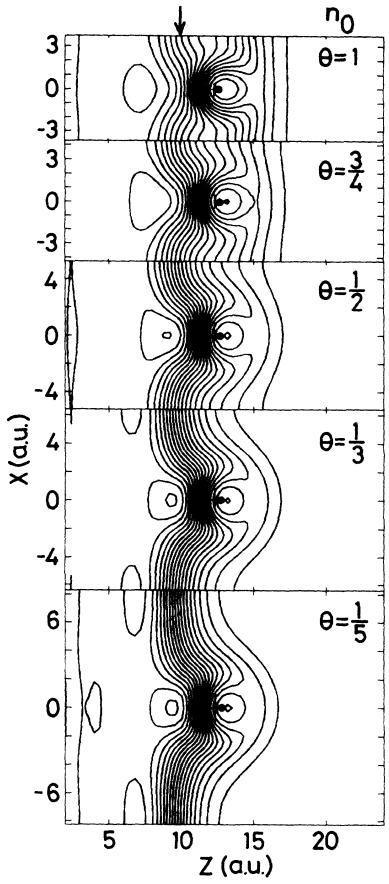

FIG. 2. Contour maps of the ground-state charge density $n_0(\mathbf{r},\Theta)$ for hexagonal Na adlayers on semi-infinite jellium with $r_s=3$ in a plane normal to the surface containing neighboring Na atoms. The contour spacing is 0.0005 a.u. The solid circles and arrow indicate the Na core and edge of the jellium substrate, respectively.

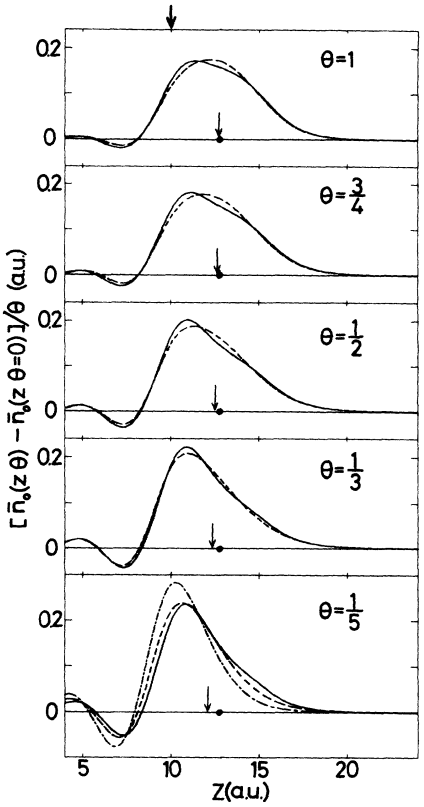

FIG. 3. Planar average of the normalized adlayer-induced ground-state charge density, $[\bar{n}_0(z,\Theta)-\bar{n}_0(z,\Theta=0)]/\Theta$ for hexagonal Na adlayers (solid curves) and thin jellium adlayers (dashed curves). The solid curves and thick arrow indicate the Na core and edge of the jellium substrate, respectively. The centroids $z_0(\Theta)$ of the solid curves are marked by thin vertical arrows. The dot-dashed curve in the lowest panel shows the density induced at the clean substrate surface by an external electric field.

transferred to the metal.[32] However, because of the appreciable width of this charge distribution, it is actually more appropriate to describe it as highly polarized chemisorption state.[18–20] Towards higher Θ, the electron distribution becomes more symmetric and its centroid shifts closer to the Na nuclei as a result of the electrostatic attraction to the more closely spaced neighboring positive Na ions. Thus, the degree of polarization of the Na atoms at large values of Θ is greatly reduced.

Also shown in Fig. 3 are the adlayer-induced charge distributions obtained for the jellium-on-jellium model. As expected, these densities are slightly more slanted towards the substrate because some of the positive ionic charge of the Na atoms is displaced towards the adlayer-substrate interface whereas in the discrete lattice it is concentrated more at the positions of the Na nuclei. For the same coverages as above, the centroids of these screening clouds are located at 0.98, 0.53, 0.27, 0.12, and 0.06 a.u., respectively. Apart from this inward shift, these distributions agree remarkably well with those of the discrete Na lattice even at low Θ.

The centroid location $z_0(\Theta)$ of the Na valence-charge distribution is of direct relevance for the Θ dependence of the work-function change, which is given as $\Delta\Phi(\Theta)=4\pi\Theta z_0(\Theta)/A$, where $A=47.4$ a.u. is the area of the unit cell at $\Theta=1$. The solid curve in Fig. 4 shows the calculated work function of the hexagonal Na adlayer as a function of Θ. It reproduces the well-known behavior, i.e., a rapid decrease at small Θ, which is followed by a minimum and a subsequent weaker rise at higher Θ. The dashed curve shows the corresponding work function for the two-step jellium model. The difference between those two curves becomes larger for lower Θ. At $\Theta=\frac{1}{5}$, the jellium adlayer overestimates $\Delta\Phi(\Theta)$ by 0.5 eV, which signifies that the jellium model overestimates the ionic nature of the adlayer at lower Θ. This is to be expected because the ionization energy of a real Na atom is 5.1 eV, whereas the jellium slab cannot bind any electrons in the low Θ limit.

Next we calculate the adatom density of states (DOS),[33]

$$\rho_a(\varepsilon,\Theta)=-\frac{1}{\pi}\int\frac{2d\mathbf{k}}{(2\pi)^2}\int_R d\mathbf{r}\,\mathrm{Im}[G(\mathbf{r},\mathbf{r},\varepsilon,\mathbf{k},\Theta,0)-G(\mathbf{r},\mathbf{r},\varepsilon,\mathbf{k},0,0)]\,, \tag{10}$$

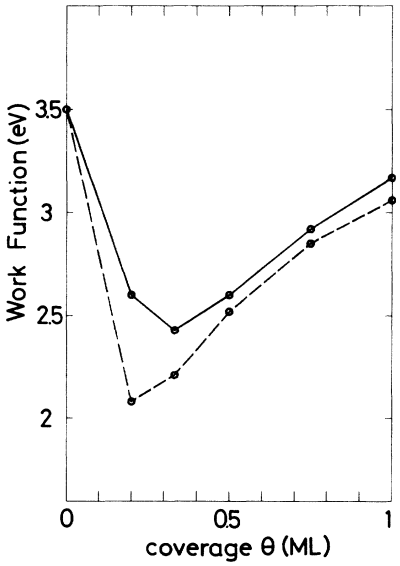

FIG. 4. Work-function $\Phi(\Theta)$ for hexagonal Na adlayers (solid lines) and thin jellium adlayers (dashed lines) as a function of coverage Θ.

where the integration over $\mathbf{r}$ is done within a sphere around a Na atom. Its radius R is chosen as 3.5 a.u. for all Θ. The calculated $\rho_a(\varepsilon,\Theta)$ which is shown in Fig. 5(a), is seen to exhibit, at low Θ, two atomiclike peaks above E_F. The lower one is a hybridized state of Na $3s$ and $3p_z$ and the higher one is due to $3p_x$ and $3p_y$. These atomic peaks are rapidly smeared out for $\Theta \geq \frac{1}{2}$ because of the formation of wide adlayer bands due to the orbital overlap between nearby adatoms. The broadening of the peaks in $\rho_a(\varepsilon,\Theta)$ does not imply disappearance of resonances, they are still sharp if $\rho_a(\varepsilon,\Theta)$ is decomposed into the $\mathbf{k}$ space. The bandwidth of the lowest hybridized s-p_z band along the $\bar{\Gamma}$-$\bar{M}$ line in the hexagonal Brillouin zone[21] is 0.7, 1.4, 2.5, and 3.6 eV for $\Theta=\frac{1}{3}$, $\frac{1}{2}$, $\frac{3}{4}$, and 1, respectively. The filled part of $\rho_a(\varepsilon,\Theta)$ is remarkably independent of Θ except at $\Theta > \frac{1}{2}$ where the larger orbital overlap among nearby atoms begins to increase $\rho_a(\varepsilon,\Theta)$ below E_F. [The filled part of $\rho_a(\varepsilon,\Theta)$ corresponds to $\sim$0.43 electrons for $R=3.5$ a.u. which agrees with the valence charge of the free atom within the same sphere.] Qualitatively, one may therefore say that the overall charge state of the chemisorbed Na atoms is rather insensitive to Θ.

The polarization rearrangement of the Na valence charge within this sphere can be seen more clearly by calculating the dipole DOS $\mu_a(\varepsilon,\Theta)$ which is defined in the same way as $\rho_a(\varepsilon,\Theta)$ except for an extra factor of $(z-z_a)$ in the volume integral of Eq. (10). The calculated $\mu_a(\varepsilon,\Theta)$ is shown in Fig. 5(b). The positive (negative) sign of $\mu_a(\varepsilon,\Theta)$ indicates polarization of the one-electron state toward the interface (vacuum) side, and thus the state can be regarded as a bonding (antibonding) state regarding the adatom-substrate bonding. It is seen that the unoccupied portion of the hybridized s,p_z state at low Θ is an antibonding state whose wave function is strongly polarized toward the vacuum side of the Na atoms. It will later be shown that this antibonding resonance above E_F at low Θ plays a crucial role for the surface response, since the virtual excitations from the occupied bonding states to this antibonding resonance have large dipole matrix elements.

In the Gurney model,[32] the energy of the partially filled adatom valence orbital shifts downwards with increasing coverage as a result of the dipole-dipole interaction. This shift may be written as[34] $\Delta\varepsilon_s(\Theta)=dE_0$, where $E_0=U\mu(\Theta)$ is the local electric field at an adatom site and $U\approx 18(\Theta/\mathrm{A})^{3/2}$ is the dipole sum for an ordered lattice. Thus, $\Delta\varepsilon\approx 2.22\Theta^{3/2}z_0(\Theta)$. At $\Theta=\frac{1}{5}$ and $\frac{1}{3}$, we, therefore, get 0.12 and 0.19 eV, respectively.

Figures 5(c) and 5(d) show the calculated $\rho_a(\varepsilon,\Theta)$ and $\mu_a(\varepsilon,\Theta)$ for the jellium adlayers. The amplitude of these functions calculated in the same sphere as for the discrete Na adlayers becomes smaller with decreasing Θ as a result of the one-dimensional nature of the model. The jellium adlayer is seen not to be able to reproduce the sharp antibonding resonance and the rapid change of sign in $\mu_a(\varepsilon,\Theta)$ at E_F at the lowest Θ; the bonding-antibonding boundary in $\mu_a(\varepsilon,\Theta)$ at $\Theta=\frac{1}{5}$ is located $\sim$0.4 eV above E_F. At higher Θ, on the other hand, the shape of these functions is qualitatively very similar to the corresponding densities of states for the discrete adlayers.

B. Linear response

Figure 6 shows contour plots of the three-dimensional linear-induced charge densities $n_1(\mathbf{r},\Theta)$ for the hexagonal Na adlayers. At all coverages, these induced densities are

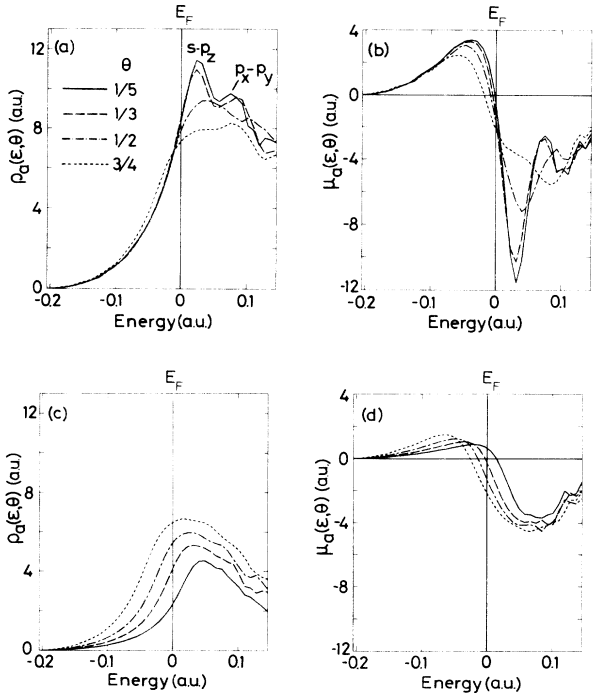

FIG. 5. (a) $\rho_a(\varepsilon,\Theta)$ and (b) $\mu_a(\varepsilon,\Theta)$ for hexagonal Na adlayers. (c) $\rho_a(\varepsilon,\Theta)$ and (d) $\mu_a(\varepsilon,\Theta)$ for thin jellium adlayers. The sphere radius R is 3.5 a.u. for all Θ.

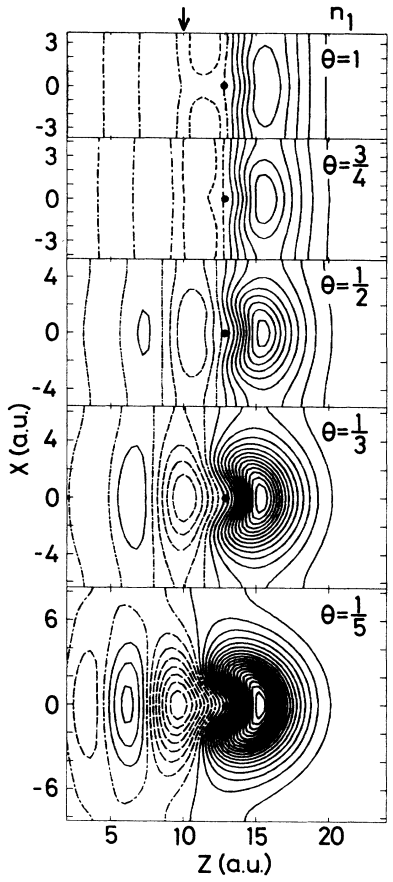

FIG. 6. Contour maps of the linear-induced charge density $n_1(\mathbf{r},\Theta)$ for hexagonal Na adlayers on semi-infinite jellium in the same plane as in Fig. 2. The solid, dashed, and dot-dashed contour lines correspond to positive, negative, and zero values of $n_1(\mathbf{r},\Theta)$, respectively. The contour spacing is 0.05 a.u.

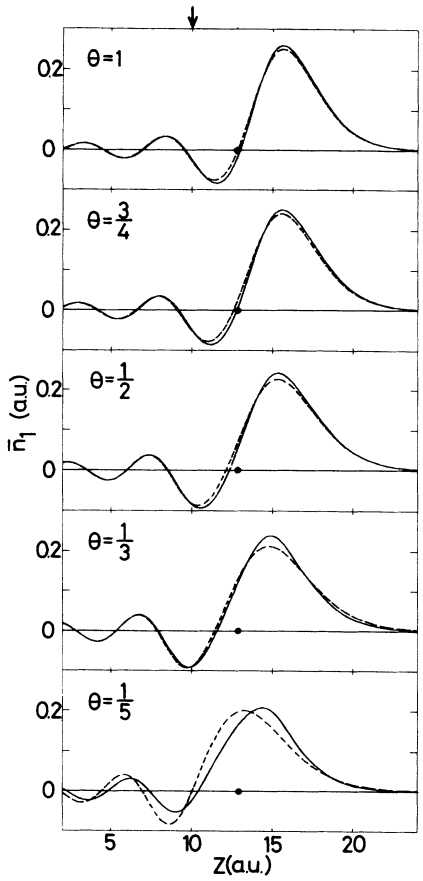

FIG. 7. Planar average of the linear-induced charge density $n_1(\mathbf{r},\Theta)$ for hexagonal Na adlayers (solid curves) and thin jellium adlayers (dashed curves). The solid circles and arrow indicate the Na core and edge of the jellium substrate, respectively.

located almost entirely on the vacuum side of the plane of Na nuclei. This reflects the efficient screening of the applied field due to the Na valence electrons. At $\Theta=1$, $n_1(\mathbf{r},\Theta)$ shows extremely weak corrugations in the planar direction, whereas with decreasing Θ, it becomes more and more atomiclike and localized within a Na atomic sphere. The peak values of $n_1(\mathbf{r},\Theta)$ are 0.28, 0.32, 0.44, 0.72, and 1.04 for $\Theta=1$, $\frac{3}{4}$, $\frac{1}{2}$, $\frac{1}{3}$, and $\frac{1}{5}$, respectively. The increase of $n_1(\mathbf{r},\Theta)$ near the adatoms leads to its depletion in the surrounding area because of the constraint Eq. (8); at $\Theta=\frac{1}{5}$, the amplitude of $n_1(\mathbf{r},\Theta)$ in the Na—Na bond region is only ~ 0.08 a.u.

The planar averages of the linear-induced charge densities are shown in Fig. 7. According to Eq. (8), the area under these curves should be unity regardless of Θ. In the present calculation, its deviation from unity in the embedded region was in most cases $\sim 1\%$ and at worst $\leq 2\%$. Thus the effect due to the tail of $n_1(\mathbf{r},\Theta)$ for $z \leq b_1$, which is treated only approximately in the embedding method, is small. The dashed curves show the corresponding induced densities for the jellium-on-jellium model, $n_1^{\text{jel}}(z,\Theta)$, which is one-dimensional from the beginning. Except for $\Theta=\frac{1}{5}$, the agreement with the solid curves is surprisingly good. Although the three-dimensional distribution of $n_1(\mathbf{r},\Theta)$ at lower Θ is far from that of the jellium adlayer, the positions and shapes of the lateral averages are nearly identical. As a result of the efficient screening, the induced density for the full monolayer nearly coincides with that induced at the surface of a semi-infinite jellium with $r_s=4$.[31]

The solid and dashed lines in Fig. 8 show the Θ dependence of the centroid of $n_1(\mathbf{r},\Theta)$,

$$z_1=\frac{1}{S}\int d\mathbf{r}\, z n_1(\mathbf{r},\Theta)\ , \tag{11}$$

for the Na adlayer, $z_1(\text{Na},\Theta)$ and for the jellium adlayer, $z_1(\text{jellium},\Theta)$, respectively. z_1 gives the position of the classical image plane. The calculated $z_1(\text{Na},\Theta)$ shifts rapidly outward at lower Θ from the value for the jellium with $r_s=3$, and saturates for $\Theta \geq \frac{1}{2}$. At $\Theta=1$, $z_1(\text{jellium},\Theta)$ agrees with the image plane position of semi-infinite jellium with $r_s=4$.[31] Since the electronic structure of Na atoms at low Θ is only weakly affected by neighboring ones, $z_1(\text{Na},\Theta)$ can be written as $z_1(\text{Na},\Theta)=(1-S_aM_a/S)z_b+(S_aM_a/S)z_a$, where z_b is z_1 for the clean surface, M_a is the number of adatoms, S_a is

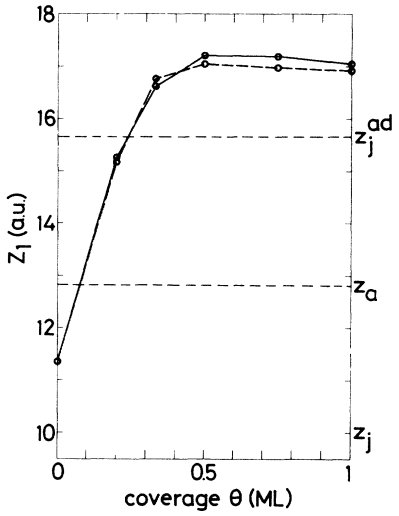

FIG. 8. Centroid z_1 of $n_1(\mathbf{r},\Theta)$ for Na adlayers (solid lines) and thin-jellium adlayers (dashed lines) as a function of Θ. The two horizontal dashed lines indicate z_a and the edge of the positive background of the jellium adlayers, z_j^{ad}.

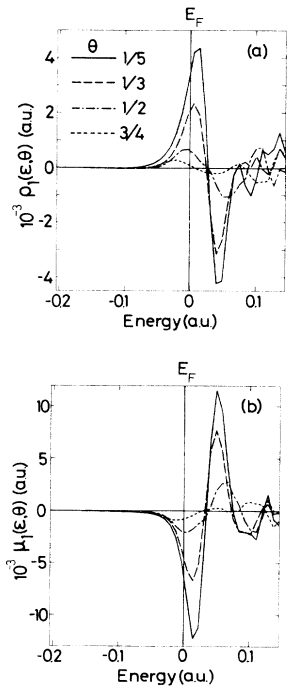

FIG. 9. (a) $\rho_1(\varepsilon,\Theta)$ and (b) $\mu_1(\varepsilon,\Theta)$ for hexagonal Na adlayers.

the area where the screening charge of a clean surface is modified by the adsorption of a single Na atom, and z_a is the centroid of the screening charge in the area of S_a. Thus at low Θ, $z_1(\mathrm{Na},\Theta)$ increases in proportion to M_a, i.e., Θ. The difference between $z_1(\mathrm{Na},\Theta)$ and $z_1(\mathrm{jellium},\Theta)$ is less than 0.2 a.u. in the whole Θ range. The agreement for $\Theta \geq \frac{1}{2}$ is not unexpected since the outermost density contours of the Na layers are nearly parallel to the surface as pointed out above (see Fig.2). On the other hand, the increase of $z_1(\mathrm{jellium},\Theta)$ at low Θ reflects the linear increase of the jellium density $n_j(\Theta)$. Its physical meaning is, therefore, not the same as that of $z_1(\mathrm{Na},\Theta)$.

The kidney-shaped contours of the localized peak on the vacuum side of a Na atom in Fig. 6 remind us of the antibonding resonance above E_F at lower Θ. As explained in Sec. III A, its wave function is strongly polarized toward the vacuum side of the adatoms, and thus virtual excitations to this resonance may give rise to such a peculiar induced charge. To examine this effect more quantitatively, we show in Fig. 9(a) the linear-induced adatom DOS defined by

$$\rho_1(\varepsilon,\Theta)=-\frac{1}{2\pi\sigma}\int\frac{2d\mathbf{k}}{(2\pi)^2}\int_R d\mathbf{r}\,\mathrm{Im}[G(\mathbf{r},\mathbf{r},\varepsilon,\mathbf{k},\Theta,\sigma)-G(\mathbf{r},\mathbf{r},\varepsilon,\mathbf{k},\Theta,-\sigma)]. \tag{12}$$

The area of $\rho_1(\varepsilon,\Theta)$ below E_F gives the amount of $n_1(\mathbf{r},\Theta)$ in the atomic sphere of radius R. The calculated values for $R=3.5$ a.u. are 7.7, 9.4, 16.5, 36.9, and 66.9 for $\Theta=1$, $\frac{3}{4}$, $\frac{1}{2}$, $\frac{1}{3}$, and $\frac{1}{5}$, respectively. In the perturbative approach, $\rho_1(\varepsilon,\Theta)$ is given by,

$$\rho_1(\varepsilon,\Theta)=\frac{-1}{\pi}\mathrm{Im}\int\frac{2d\mathbf{k}}{(2\pi)^2}\int_R d\mathbf{r}\int d\mathbf{r}'\,G(\mathbf{r},\mathbf{r}',\varepsilon,\mathbf{k},\Theta,0)v_1(\mathbf{r}')G(\mathbf{r}',\mathbf{r},\varepsilon,\mathbf{k},\Theta,0)$$
$$=\sum_{\varepsilon'}\frac{1}{\varepsilon-\varepsilon'}\left[\langle\phi_{\varepsilon'}|v_1|\phi_\varepsilon\rangle\int_R d\mathbf{r}\,\phi_\varepsilon^*\phi_{\varepsilon'}+\mathrm{c.c.}\right]. \tag{13}$$

Here ϕ_ε denotes the wave function of the one-electron state with energy ε in the ground state, and $v_1=[v_0(\mathbf{r},\Theta,\sigma)-v_0(\mathbf{r},\Theta,-\sigma)]/(2\sigma)$, where $v_0(\mathbf{r},\Theta,\sigma)$ is the effective one-electron potential for the Kohn-Sham equation. The calculated $\rho_1(\varepsilon,\Theta)$ at lower Θ changes its sign rapidly at the peak energy of the antibonding resonance (ε_a). Its ε dependence can be essentially understood as $\mathrm{Re}[1/(\varepsilon-\varepsilon_a-i\Gamma_a)]$, i.e., the energy denominator in the second line of Eq. (13), except for the higher ε range where the second resonance (p_x and p_y) becomes important. This is a clear evidence showing the importance of the antibonding resonance for the surface response at lower Θ. The increase in the amplitude of $\rho_1(\varepsilon,\Theta)$ below E_F with decreasing Θ reflects the matrix element in Eq. (13), $\int d\mathbf{r}\,\phi_\varepsilon^*\phi_{\varepsilon_a}$, since the wave function of the antibonding resonance is more and more localized

on the vacuum side of Na with decreasing Θ.

Figure 9(b) shows the linear-induced dipole DOS, $\mu_1(\varepsilon,\Theta)$, which is defined in the same way as $\rho_1(\varepsilon,\Theta)$ except for an additional factor, $z-z_a$, in the $\mathbf{r}$ integration just as in the case of $\mu_a(\varepsilon,\Theta)$. Its expression in the perturbation theory is given by replacing $\int_R d\mathbf{r}\,\phi_\varepsilon^*\phi_{\varepsilon'}$ in Eq. (13) by $\int_R d\mathbf{r}\,\phi_\varepsilon^*(z-z_a)\phi_{\varepsilon'}$. Thus $\mu_1(\varepsilon,\Theta)$ shows similar ε and Θ dependences as $\rho_1(\varepsilon,\Theta)$. The virtual excitation to the antibonding resonance gives a large negative matrix element $\int_R d\mathbf{r}\,\phi_\varepsilon^*(z-z_a)\phi_{\varepsilon_a}$, which makes $\mu_1(\varepsilon,\Theta)$ negative below E_F.

C. Nonlinear response

Figure 10 shows contour maps of the second-order induced density $n_2(\mathbf{r},\Theta)$ for the hexagonal Na adlayers. As in the case of $n_1(\mathbf{r},\Theta)$, $n_2(\mathbf{r},\Theta)$ is only weakly corrugated for a full Na adlayer but becomes more and more localized around the Na atoms with decreasing Θ. The amplitude of the positive peak on the vacuum side of Na at $\Theta=\frac{1}{5}$ is ~ 280 a.u., which is more than nine times larger than that of the corresponding maximum at $\Theta=1$. Next to this positive peak, there is a region of negative $n_2(\mathbf{r},\Theta)$, which has two minima and thus spacially has a ringlike shape. The two minima shift from the interface to the vaccum side of the Na plane with increasing Θ.

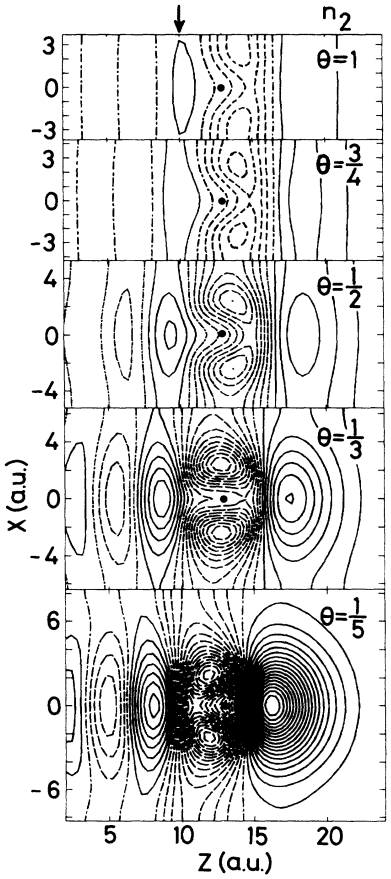

FIG. 10. Contour maps of the nonlinear-induced charge density $n_2(\mathbf{r},\Theta)$ for hexagonal Na adlayers on semi-infinite jellium in the same plane as in Fig. 2. The solid, dashed, and dot-dashed contour lines correspond to positive, negative, and zero values of $n_2(\mathbf{r},\Theta)$, respectively. The contour spacing is 15 a.u.

The solid curve in Fig. 11 show the planar averages of $n_2(\mathbf{r},\Theta)$ for the hexagonal Na adlayers of jellium, $\bar{n}_2(z,\Theta)$. The calculated $\bar{n}_2(z,\Theta)$ has a positive peak on the vacuum side of the Na layer, a second negative peak with the largest amplitude, and subsequent smaller Friedel oscillations in the bulk. The first peak is located 2–3 a.u. farther on the vacuum side than the main peak of $\bar{n}_1(z,\Theta)$. The dashed curves in Fig. 11 show the nonlinear-induced charge density of the jellium adlayers, $n_2^{\rm jel}(z,\Theta)$. As in the case of the linear response, the agreement between $\bar{n}_2(z,\Theta)$ and $n_2^{\rm jel}(z,\Theta)$ is excellent for $\Theta\geq\frac{1}{2}$, which suggests that the present choice of parameters for the jellium adlayer is realistic. At lower coverages, the differences become progressively more pronounced because of the extreme atomic character of the three-dimensional nonlinear charge densities.

According to Weber and Liebsch,[30] at low frequencies (ω), the long-wavelength limit of the longitudinal second-harmonic (SH) current is given by

$$j_{2\omega}(z)=\omega E_{apl}^2 P_2(z)/(4\pi)^2\ , \tag{14}$$

with

$$P_2(z)=-\int_z^\infty dz'\bar{n}_2(z',\Theta)\ . \tag{15}$$

The current due to a component of $n_2(\mathbf{r},\Theta)$ with nonzero $\mathbf{G}$ vectors does not generate an electric field propagating into the vacuum, and thus only the long-wavelength component (planar average) is observable. The polarizations $P_2(z)$ for the Na adlayers, which give a direct picture of the shape of the surface current, are shown in Fig. 12 by the solid curves. The dashed curves show the results for the jellium adlayers. The calculated $P_2(z)$ have a main

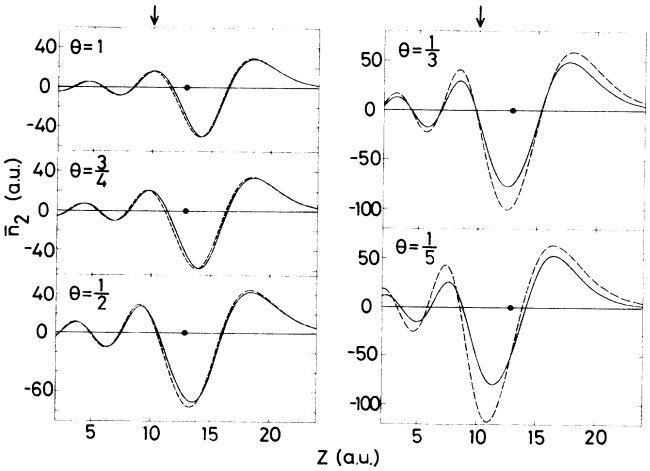

FIG. 11. Planar average of the nonlinear-induced charge density $n_2(\mathbf{r},\Theta)$ for hexagonal Na adlayers (solid curves) and thin jellium adlayers (dashed curves).

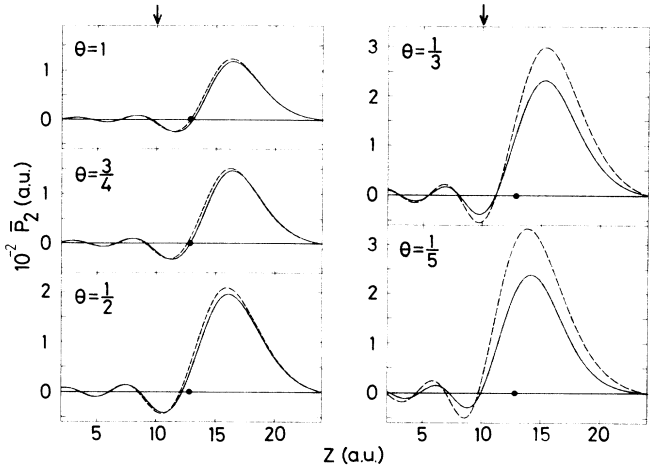

FIG. 12. Nonlinear polarization $P_2(z)$ for hexagonal Na adlayers (solid curves) and thin jellium adlayers (dashed curves).

peak on the vacuum side of the Na plane and subsequent Friedel oscillations. The position of the main peak shifts inward with decreasing Θ just as the peak positions of $\bar{n}_2(z,\Theta)$. The locations and shapes of these polarizations are seen to be in excellent agreement for the discrete and jellium adlayers. The main difference is the peak height which at low Θ is overestimated in the jellium model. At $\Theta=1$, the curves nearly coincide with the nonlinear polarization induced at a semi-infinite jellium with $r_s=4$.[30]

Figure 13 shows the integrated weights p_2 of these second-order polarization distributions defined by

$$p_2=\int dz\, P_2(z)=-\frac{1}{S}\int d\mathbf{r}\, z n_2(\mathbf{r},\Theta) \tag{16}$$

for the Na (solid lines) and jellium (dashed lines) adlayers.

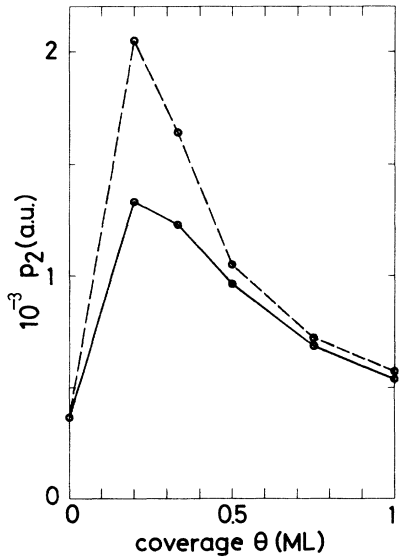

FIG. 13. Θ dependence of p_2 for hexagonal Na adlayer (solid lines) and thin jellium adlayers (dashed lines).

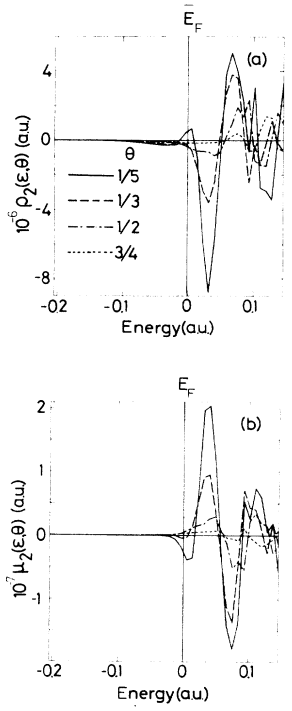

FIG. 14. (a) $\rho_2(\varepsilon,\Theta)$ and (b) $\mu_2(\varepsilon,\Theta)$ for hexagonal Na adlayers.

p_2 is related to the dimensionless parameter a introduced by Rudnick and Stern[35] as a measure of the longitudinal part of the SH surface current.[36–38] At low frequencies, $a=4n_{\text{sub}}p_2$,[30] where n_{sub} is the electron density of the substrate. The agreement between the Na and jellium adlayers is very good for $\Theta\geq\frac{1}{2}$, while for lower Θ the jellium adlayer overestimates p_2 substantially. Both for the Na and jellium adlayers, the calculated p_2 shows a rapid increase at lower Θ from the value of the bare substrate, and takes a maximum. At $\Theta=\frac{1}{5}$, the SHG efficiency of the Na adlayer, which is proportional to p_2^2, is 13.3 times larger than that of the clean substrate. The enhancement of p_2 for the jellium adlayer stems from the decrease in the effective surface electron density due to the adlayer. Weber and Liebsch[30] showed that the p_2 value of clean jellium surfaces increases with the decreasing surface electron density. The enhancement of p_2 for the Na adlayer at lower Θ, on the other hand, reflects the large nonlinear polarizability of Na adatoms. Thus its origin is different from that for the jellium adlayer.

In the present calculation, p_2 diminishes for $\Theta\geq\frac{1}{5}$, while the SH signal increased monotonically up to the full monolayer Θ in the recent experiment of Song *et al.*[10] for Rb/Ag. The enhancement for the full monolayer was very large, and its amplitude depended on the incident laser frequency. These may be due to the dynamical effects which cannot be taken account of in the present static calculation. Recently, Liebsch[13] studied the dynamical response of alkali-metal monolayers using the jellium-adlayer model. He showed that the SHG efficiency is greatly enhanced when the harmonic fre-

quency approaches the frequency of a collective mode at the adlayer-vacuum interface. Unless interband transitions play an important role, these results may be quite reliable since the present work shows that the jellium model for the adlayer is adequate as long as $\Theta \geq \frac{1}{2}$.

To conclude this section, we show in Fig. 14(a) the nonlinear-induced adatom DOS defined by

$$\rho_2(\varepsilon,\Theta)=-\frac{1}{2\pi\sigma^2}\int\frac{2d\mathbf{k}}{(2\pi)^2}\int_R d\mathbf{r}\,\mathrm{Im}[G(\mathbf{r},\mathbf{r},\varepsilon,\mathbf{k},\Theta,\sigma)+G(\mathbf{r},\mathbf{r},\varepsilon,\mathbf{k},\Theta,-\sigma)-2G(\mathbf{r},\mathbf{r},\varepsilon,\mathbf{k},\Theta,0)]\ . \tag{17}$$

In the perturbation theory, $\rho_2(\varepsilon,\Theta)$ is given as

$$\rho_2(\varepsilon,\Theta)=-\frac{1}{\pi}\mathrm{Im}\int\frac{2d\mathbf{k}}{(2\pi)^2}\int_R d\mathbf{r}\int d\mathbf{r}'\,G(\mathbf{r},\mathbf{r}',\varepsilon,\mathbf{k},\Theta,0)v_2(\mathbf{r}')G(\mathbf{r}',\mathbf{r},\varepsilon,\mathbf{k},\Theta,0)$$
$$-\frac{1}{\pi}\mathrm{Im}\int\frac{2d\mathbf{k}}{(2\pi)^2}\int_R d\mathbf{r}\int d\mathbf{r}'d\mathbf{r}''\,G(\mathbf{r},\mathbf{r}',\varepsilon,\mathbf{k},\Theta,0)v_1(\mathbf{r}')$$
$$\times G(\mathbf{r}',\mathbf{r}'',\varepsilon,\mathbf{k},\Theta,0)v_1(\mathbf{r}'')G(\mathbf{r}'',\mathbf{r},\varepsilon,\mathbf{k},\Theta,0)\ , \tag{18}$$

where $v_2=[v_0(\mathbf{r},\Theta,\sigma)+v_0(\mathbf{r},\Theta,-\sigma)-2v_0(\mathbf{r},\Theta,0)]/(2\sigma^2)$. The second term in Eq. (18) is a driving term to the nonlinear response, while the first one is a screening term which fulfills the constraint Eq. (9). Because these two terms show different ε dependence, the interpretation of the calculated $\rho_2(\varepsilon,\Theta)$ is not as direct as that of $\rho_1(\varepsilon,\Theta)$. In the energy range between E_F and the onset of the p_x (p_y) resonance, $\rho_2(\varepsilon,\Theta)$ appears similar to the energy derivative of $\rho_1(\varepsilon,\Theta)$; for example, the positions of two large peaks in $\rho_1(\varepsilon,\Theta)$ at $\Theta=\frac{1}{5}$ coincide fairly well with two zero points in $\rho_2(\varepsilon,\Theta)$. This may be qualitatively understood in terms of the second term of Eq. (18), though it becomes the exact energy derivative of $\rho_1(\varepsilon,\Theta)$ only when v_1 is constant. Figure 14(b) shows the nonlinear-induced dipole density $\mu_2(\varepsilon,\Theta)$, which is defined in the same way as $\rho_2(\varepsilon,\Theta)$ except for an extra factor, $z-z_a$, in the $\mathbf{r}$ integration. As in the case of $\mu_1(\varepsilon,\Theta)$, $\mu_2(\varepsilon,\Theta)$ shows similar ε and Θ dependences as $\rho_2(\varepsilon,\Theta)$ except that they have opposite signs.

IV. SUMMARY

Alkali-metal adlayers on metal surfaces show interesting response properties such as the appearance of a strong loss peak in electron energy-loss spectra and the enormous enhancement of the SHG efficincy. The understanding of these phenomena needs a consistent description of the transition from the atomiclike response at low Θ to the metallic response at high Θ. As a first step in this direction, we studied the linear and nonlinear response of the alkali-metal adlayers in the presence of a *static* electric field nonempirically. Hexagonal Na layers with varying lattice constants were used as adlayers, and the metal substrate was modeled by a semi-infinite jellium with $r_s=3$. For coverages below the work-function minimum, the response is atomiclike. This atomic character becomes progressively more pronounced as we go from ground state to linear-induced to nonlinear-induced charge densities. The virtual excitation from the occupied bonding states to the antibonding resonance above E_F, which is a hybridized state of the valence s and p_z states, plays a dominant role in these surface response properties.

A surprising and important result of the present work is the finding that, despite the prominent atomiclike shape of the three-dimensional densities, their planar averages agree remarkably well with the corresponding density distributions obtained within the one-dimensional jellium-on-jellium model. Only at coverages below the work function do the differences become appreciable. The extension of the present work to the dynamical response within the time-dependent density-functional theory requires the construction of linear and nonlinear surface response functions, based on the one-electron Green functions of the ground-state employed in the present scheme. Such a study is now under way.

ACKNOWLEDGMENTS

We are indebted to Dr. S. Blügel for allowing us to use his convergence method before publication. One of the authors (H.I.) thanks the Forschungszentrum Jülich for its support during his stay at Jülich, where most of the work was completed.

[1]H. P. Bonzel, Surf. Sci. Rep. **8**, 43 (1987).

[2]*Physics and Chemistry of Alkali Metal Adsorption*, edited by H. P. Bonzel, A. M. Bradshaw, and G. Ertl (Elsevier, Amsterdam, 1989).

[3]T. Aruga and Y. Murata, Prog. Surf. Sci. **31**, 61 (1989).

[4]D. Heskett, K.-H. Frank. K. Horn, E. E. Koch, H.-J. Freund, A. Baddorf, K.-D. Tsuei, and E. W. Plummer, Phys. Rev. B **37**, 10 387 (1988); U. Jostell, Surf. Sci. **82**, 333 (1979); T. Aruga, H. Tochihara, and Y. Murata, Phys. Rev. B **34**, 8237 (1986).

[5]J. Cousty, R. Riwan, and P. Soukiassian, J. Phys. (Paris) **46**, 1693 (1985).

[6]A. Hohlfeld, M. Sunjic, and K. Horn, J. Vac. Sci. Technol. A **5**, 679 (1987).
[7]H. Ishida and M. Tsukada, Surf. Sci. **169**, 225 (1986).
[8]A. G. Eguiluz and A. Campbell, Phys. Rev. B **31**, 7572 (1985); J. E. Inglesfield and E. Wirkborg, J. Phys. F **5**, 1706 (1975); D. M. Newns, Phys. Lett. **39A**, 341 (1972).
[9]H. W. K. Tom, C. M. Mate, X. D. Zhu, J. E. Crowell, Y. R. Shen, and G. A. Somorjai, Surf. Sci. **172**, 466 (1986).
[10]K. J. Song, D. Heskett, H. L. Dai, A. Liebsch, and E. W. Plummer, Phys. Rev. Lett. **61**, 1380 (1988).
[11]B. N. J. Persson and L. H. Dubois, Phys. Rev. B **39**, 8220 (1989).
[12]J. P. Muscat and D. M. Newns, J. Phys. C **7**, 2630 (1974); J. P. Muscat and I. P. Batra, Phys. Rev. B **34**, 2889 (1986).
[13]A. Liebsch, Phys. Rev. B **40**, 3421 (1989).
[14]A. Liebsch, J. Phys. C **19**, 5025 (1986); Phys. Rev. B **36**, 7378 (1987).
[15]A. Liebsch, Phys. Rev. Lett. **61**, 1233 (1988).
[16]A. Liebsch and W. L. Schaich, Phys. Rev. B **40**, 5401 (1989).
[17]A. Liebsch, G. Hincelin, and T. López-Ríos, Phys. Rev. B **41**, 10 463 (1990).
[18]H. Ishida and K. Terakura, Phys. Rev. B **36**, 4510 (1987); B **38**, 5752 (1988); B **40**, 11 519 (1989).
[19]H. Ishida, Phys. Rev. B **38**, 8006 (1988).
[20]H. Ishida, Phys. Rev. B **39**, 5492 (1989).
[21]H. Ishida, Phys. Rev. B **40**, 1341 (1989); Phys. Rev. Lett. **63**, 1535 (1989).
[22]M. Weber and A. Liebsch, Phys. Rev. B **36**, 6411 (1987).
[23]N. D. Lang, Phys. Rev. B **4**, 4234 (1971).
[24]N. D. Lang and A. R. Williams, Phys. Rev. B **18**, 616 (1978); B **16**, 2408 (1977).
[25]W. Kohn and L. J. Sham, Phys. Rev. **140**, A1133 (1965); P. Hohenberg and W. Kohn, Phys. Rev. **136**, B864 (1964).
[26]J. E. Inglesfield, J. Phys. C **14**, 3795 (1981). See also, J. E. Inglesfield, Surf. Sci. **188**, L701 (1987); G. C. Aers and J. E. Inglesfield, *ibid.* **217**, 367 (1989), where the response of clean metal surfaces to a static electric field is studied by the embedding method.
[27]The sign of the matrix element was misprinted as "positive" in Ref. 20.
[28]G. B. Bachelet, D. R. Hamann, and M. Schlüter, Phys. Rev. B **26**, 4199 (1982).
[29]S. Blügel (unpublished).
[30]M. Weber and A. Liebsch, Phys. Rev. B **35**, 4711 (1986).
[31]N. D. Lang and W. Kohn, Phys. Rev. B **7**, 3541 (1973).
[32]R. W. Gurney, Phys. Rev. **47**, 479 (1935).
[33]The second turn of Eq. (10) is the DOS for the bare jellium surface in the same atomic sphere. The definition of $\rho_a(\varepsilon,\Theta)$ coincides with that in Ref. 24 if R is large enough.
[34]B. N. J. Persson and H. Ishida, Phys. Rev. B **42**, 3171 (1990).
[35]J. Rudnick and E. A. Stern, Phys. Rev. B **4**, 4272 (1971).
[36]J. E. Sipe and G. I. Stegeman, in *Surface Polaritons,* edited by V. M. Agranovich and D. L. Mills (North-Holland, New York, 1982).
[37]M. Corvi and W. L. Schaich, Phys. Rev. B **33**, 3688 (1986).
[38]W. L. Schaich and A. Liebsch, Phys. Rev. B **37**, 6187 (1988).